arXiv:2103.09337v3 [cond-mat.mes-hall] 8 Oct 2021

Current vortices in hexagonal graphene quantum dots

Eudes Gomes * and Fernando Moraes †
Departamento de Física, Universidade Federal Rural de Pernambuco, 52171-900 Recife, PE, Brazil
(Dated: February 14, 2022)

Newly synthesized nanostructures of graphene appear as a promising breeding ground for new technology. Therefore, it is important to identify the role played by the boundary conditions in their electronic features. In this contribution we use the non-equilibrium Green's function method coupled to tight-binding theory to calculate and compare the current patterns of hexagonal graphene quantum dots, with contacts placed at different edge locations. Our results reveal the formation of current vortices when the geometry of the contact position is not centrosymmetric. That is, when they are placed on non-frontal armchair-like vertices of the quantum dot. The introduction of defects, leading to disorder, significantly alters the current behavior, distorting bulk vortices and annihilating the edge currents. Nevertheless, periodically distributed defects on the edge allow for the appearance of current loops that dodge the defects. The presence of current vortices suggests the use of graphene quantum dots as nanomagnets or magnetic nanosensors.

I. INTRODUCTION

Graphene Quantum Dots (GQD)[1] or nanoflakes, have attracted a great deal of attention due to their possible electronic[2], photonic[3] and medical[4] applications. In this article, we investigate the possibility of generating current vortices in a hexagonal GQD. The shape choice is due to two reasons. First, the hexagonal shape preserves the local symmetry of the atomic network facilitating the calculations and second, hexagonal nanographene has been recently successfully synthesized[5–7]. The possibility of having current vortices in those nanoflakes suggests interesting applications, like their use as nanomagnets or magnetic nanosensors, for instance. This is the main motivation of this work. The electronic states of hexagonal and triangular GQDs have been thoroughly explored by Zarenia and coworkers[8] and the dependence on size of the electronic structure of hexagonal GQDs was studied by[9] using density functional theory.

Current vortices in graphene have been of great interest in recent years[10,11]. They have been predicted to appear in the so-called hydrodynamic viscous regime, where electron-electron collisions are dominant (for a recent review see[12]) over electron-phonon or electron-impurity scattering. Since electron-phonon scattering is weak in graphene, as well as the degree of purity can be extremely high, the hydrodynamic behavior may be reached at reasonably low temperatures (say, above liquid nitrogen temperature). The backflow associated to the vortices in the hydrodynamic regime implies in a negative local resistance[13] giving indirect experimental evidence of their presence. This regime is not exclusive of graphene but may occur in ultra-clean 2D electron systems, as has been recently observed experimentally in a high purity GaAs quantum well[14]. Although negative resistances and current vortices seem to be characteristics of the hydrodynamic regime, they may also appear in the ballistic regime, as recently verified by Gupta and coworkers[15].

Using a simple tight-binding model we show that, even without considering electron-electron interaction, current vortices may appear in a gated hexagonal graphene quantum dot with zigzag edge, depending on the contact locations and injection energy. We start by characterizing the elementary electronic properties, such as energy spectrum and density of states, of the hexagonal structure $C_{486}H_{54}$ depicted in Fig. 1. This is done by numerical diagonalization of the tight-binding Hamiltonian, and gives good agreement with the literature. The local density of states, transmission and local current are then obtained by coupling the tight-binding results to the Non-Equilibrium Green's Function (NEGF) method. For selected contact configurations, we obtain the transmission spectrum, which then allows us to choose the relevant values for the injection energy of each configuration. For some injection energies, vortices and their associated backflows appear clearly when the contacts are placed at two non-frontal armchair vertices.

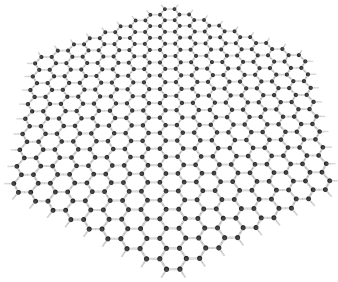


FIG. 1: Perspective view of a hexagonal graphene nanoflake $C_{486}H_{54}$. Hydrogen atoms (not shown) are attached to the atoms of the edge to avoid dangling bonds.

Ring currents have been found in an *ab initio* study of a graphene nanoribbon[16]. Circular currents have also been found in hydrocarbon molecules, including coronene which is a smaller version of the system we study here, both by more robust techniques like Kohn-Sham Density Functional Theory coupled to NEGF[17] and the simple tight-binding/NEGF[18] method we use here. This justifies[19] the use of the latter approach in our studies, suggesting that the vortices we observe should also ap-

pear in more detailed treatments.

Although our model is oversimplified, it still seems to be accurate when describing effects due to defects on the edges[20]. The presence of these defects (defect here means removal of atoms) at the edges, and even in the bulk, were analyzed, and current vortices were found on some of our structures, depending on the degree of the disorder introduced by the defects. For a detailed discussion on the role played by defects on the edges of graphene nanoribbons see[21].

A note on the nomenclature used for closed current loops is due here. While in a superfluid one might have a free vortex, that needs not an energy supply to be maintained, in this work we use the term "vortex" to designate a forced vortex, in the sense that a potential difference is needed to keep it, due to ohmic losses. These are like the forced vortices that appear upon stirring water in a kitchen pot. On the other hand, in superconducting graphene, for instance, one might have free vortices, which will persist after turning off the potential difference that originated them.

II. METHODS

A. Tight-binding calculations

The tight-binding approach for molecules uses the most relevant atomic orbitals λ associated to each atom i as a basis to construct the single particle state $|\psi\rangle = \sum_{i\lambda} |i\lambda\rangle$. In our calculations we will use only π orbitals since these are mostly responsible for the transport properties in graphene. The tight-binding Hamiltonian, written in the local π orbitals' basis, is then given by

$$H = \sum_i \varepsilon_i |i\rangle \langle i| + \frac{1}{2} \sum_{i \neq j} t_{ij} |i\rangle \langle j| , \tag{1}$$

where ε_i is the on-site orbital energy and t_{ij} is the hopping integral. Considering only first-neighbor interactions, we define the overlap matrix

$$S_{ij} = \begin{cases} 1, & \text{if } i = j \\ s, & \text{if i, j are neighbors} \\ 0, & \text{otherwise} \end{cases}$$

and the hopping matrix

$$H_{ij} = \begin{cases} \epsilon_i, & \text{if } i = j \\ t, & \text{if i, j are neighbors} \\ 0, & \text{otherwise} \end{cases}$$

and use $\epsilon_i = 0$, $t = -3.1\, eV$ and $s = 0.12$, following Ref.[22]. Our task now reduces to finding the eigenvalues E of the Hamiltonian (1) by solving the characteristic equation

$$\det(H - ES) = 0. \tag{2}$$

The hopping and overlap matrices (H, S) are easily constructed when one knows the connections among the atoms. In our case, each carbon atom is connected to another three except at the edge where the connectivity is two.

B. The Non-Equilibrium Green's Function Method

In order to obtain the transport properties of the nanoflakes, we resort to the Non-Equilibrium Green's Function (NEGF) method which, coupled to the tight-binding formalism, is well known as an excellent tool to study current flow and transport phenomena in nanostructures[19,23–27]. To use the NEGF method we need to attach to the nanostructure two or more leads, which are metallic contacts acting as reservoirs. These contacts are modeled using a square lattice (see Fig. 2) and the reservoirs are kept at different chemical potentials, keeping the whole system out of equilibrium. Each reservoir is characterized by its own Fermi distribution. We can use NEGF to calculate electronic properties such as, the local current I_{ij} between neighboring lattice sites i and j, the transmission, and the local density of states (LDOS). Since the NEGF method is widely discussed

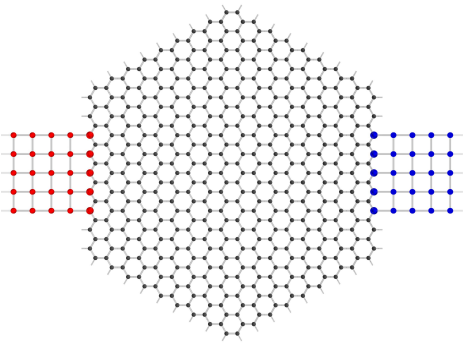


FIG. 2: Source (red) and drain (blue) contacts at the hexagonal GQD edge.

in[28,29], we summarize here only the essential concepts. We start by writing down the Green's function of the system, given by

$$G(E) = (ES - H - \Sigma_i)^{-1}, \tag{3}$$

where E is the single-particle energy of the injected electrons and S, H and Σ_i are the overlap, hopping and the so called self-energies, respectively. The self-energies account for the contacts attached to the nanoflakes, which are modeled by a semi-infinite square lattice as described in[30,31]. Besides the real contacts associated to the reservoirs, it is also possible to attach virtual contacts to the remaining edge atoms. These contacts can be placed in order to suppress boundary effects by means of an imaginary self-energy. Here, these virtual contacts are modeled using the wide-band approximation, which can be

expressed as $\Sigma^{edge} = -i\nu \sum_n |n\rangle \langle n|$, where $\nu > 0$ is a parameter[23,32]. Later on, in Subsection IV A, we shall show the role played by these virtual contacts on the transmission. In Fig. 2 we show the hexagonal GQD of interest with source (red) and drain (blue) contacts, with a few sites of the respective square lattices. The injection is modeled by an inscattering function of the form

$$\Sigma^{in} = \Gamma_s f_s + \Gamma_d f_d, \tag{4}$$

where subscripts $s(d)$ stand for source (drain) and the function $\Gamma_k = i(\Sigma_k - \Sigma_k^\dagger)$, $k = s, d$, is called broadening matrix. The functions $f_{s,d}$ are Fermi distributions for the reservoirs. With this formalism, we obtain the transport properties by means of the transmission function[19]

$$T(E) = \mathrm{Tr}\big[\mathrm{Im}(\Sigma_s) G \,\mathrm{Im}(\Sigma_d) G^\dagger\big], \tag{5}$$

as well as the local current between atoms i and j,

$$I(E)_{ij} = \frac{2e}{h} \,\mathrm{Im}(H_{ij}^* G_{ij}^n), \tag{6}$$

where $G^n = G\Sigma^{in}G^\dagger$ is the correlation function[23,29]. Another important information that we can obtain from the Green's function method is the local density of states, which is given by[28]

$$\rho(E, i) = -\frac{1}{\pi} \,\mathrm{Im}(G_{ii}(E)). \tag{7}$$

When studying the nanoflake without contacts, we write the Green's function as

$$G(E) = \left[(E + i\mu)S - H\right]^{-1}, \tag{8}$$

where $\mu > 0$ is a parameter and $i = \sqrt{-1}$. All relevant results in this work were obtained by means of the above equations coupled to the tight-binding model described in the previous subsection. We used the value $\mu = 0.0025\, eV$. For more information on the role of the parameter, μ see[33]. Equation (8) will be used to evaluate the LDOS without any influence of the contacts. To evaluate the LDOS taking into account the presence of the contacts, we can use the complete Green's equation given by (3). The code to perform the calculations was written in Python, and for the visualization of the LDOS and current patterns we used Mayavi[34].

III. RESULTS

A. Energy spectrum and density of states

As a verification of our method, we performed the electronic characterization of the hexagonal GQD and compared it to known results for similar structures. In Fig. 3 we show the energy spectrum, as obtained from the diagonalization of Eq. (2), and the corresponding Gaussian broadened (full width at half maximum = $0.3\, eV$) Density of States (DOS). The overall shape and major peaks

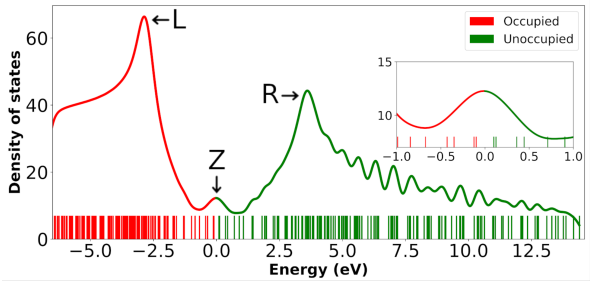


FIG. 3: Density of States and energy spectrum for the hexagonal graphene quantum dot. Red (green) indicates occupied (unoccupied) states. The letters L,R,Z indicate the position of the two van Hove and zero states, respectively. The corresponding energy values are $L = -2.8685\, eV$, $R = 3.6014\, eV$ and $Z = 0.0\, eV$. The inset shows the states around Z.

of the DOS, correspond to the ones obtained previously in the literature[35,36] for comparable structures. Note the presence of the peak at zero energy in the DOS (indicated by Z in Fig. 3). As it is well known[37], zero modes in 2D

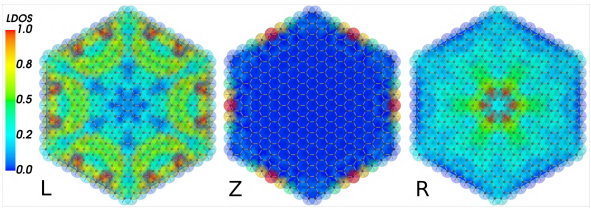
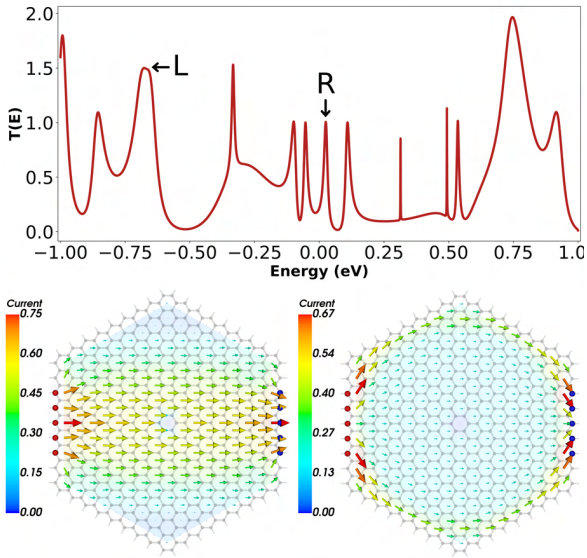


FIG. 4: Local Density of States corresponding to the three selected DOS peaks in Fig. 3. Note the edge states in the central illustration (Z) corresponding to the zero modes.

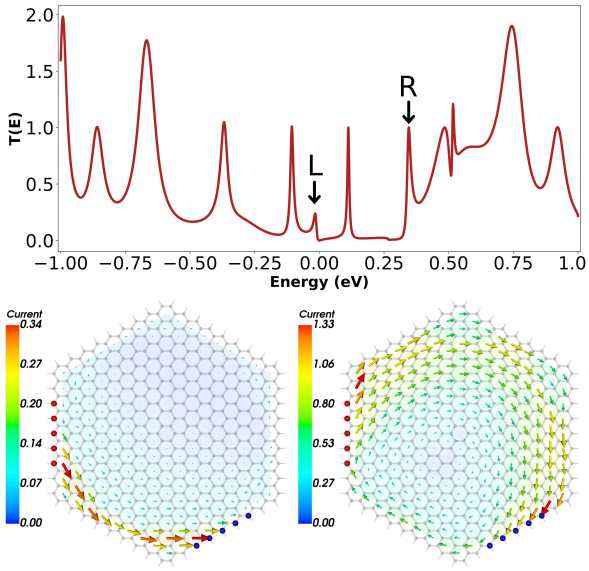
carbon structures correspond to edge states, as confirmed by the map of the Local Density of States (LDOS) at zero energy (Fig. 4 Z) on the structure. This is in close agreement with the results of Ref.[35] for the Highest Occupied Molecular Orbital (HOMO) and of Ref.[9] for the Lowest Unoccupied Molecular orbital (LUMO) of zigzag hexagonal carbon nanoflakes. To be precise, there is no zero energy state for this structure but the HOMO and LUMO states, which are symmetrically placed around zero, with a gap of nearly $0.2\, eV$. As verified in Ref.[9], increasing the size of the structure reduces the gap, eventually leading to its closure in the infinite graphene limit. The LDOS at the van Hove peaks reflect the common symmetries of the hexagonal lattice and the edge shape, as can be seen in Fig. 4, for the first (left) and for the second (right) peak. A detailed study of the effects on the van Hove peaks due to defects or edge shape in flat graphene nanoflakes can be found in Ref.[38] and the consequences for optical properties in[39].

B. Transmission and current

The total transmission as a function of the energy can be obtained from equation (5), but note that it also depends on the leads configuration.



(a) Top: transmission as a function of injection energy for the contact configuration shown in Fig. 2.



(b) Top: transmission as a function of injection energy for contacts placed on two non-adjacent edges of the hexagonal GQD.

FIG. 5: Bottom of each figure: current patterns corresponding to the selected transmission peaks, L (left) and R (right). The color bar presents a scale for the current intensity in units of $\frac{2e}{h}$. Contacts are represented by colored dots: source (red) and drain (blue).

We start by analyzing the configuration presented in Fig. 2, with contacts placed on opposing edges. In the upper part of Fig. 5a we show the transmission as function of injection energy for this configuration. In the lower part, we show the current patterns for two selected values of injection energy. A note on the current diagrams: each arrow, except those in the central polygon when they appear, is the resulting sum over the currents at the edges of each polygon in the structure. The current patterns shown in Fig. 5a are representative of what is obtained at the other transmission peaks: the current leaves the source and goes to the drain with some lateral spreading whose degree varies with the injection energy. The closer the injection energy is to zero, the greater the spreading until the current goes mostly through the edge states (compare with Fig. 4 Z). Obviously, the symmetric arrangement of the contacts across the sample does not favor a circular current pattern formation. As it will be seen next, this happens when the contacts are placed asymmetrically across the flake.

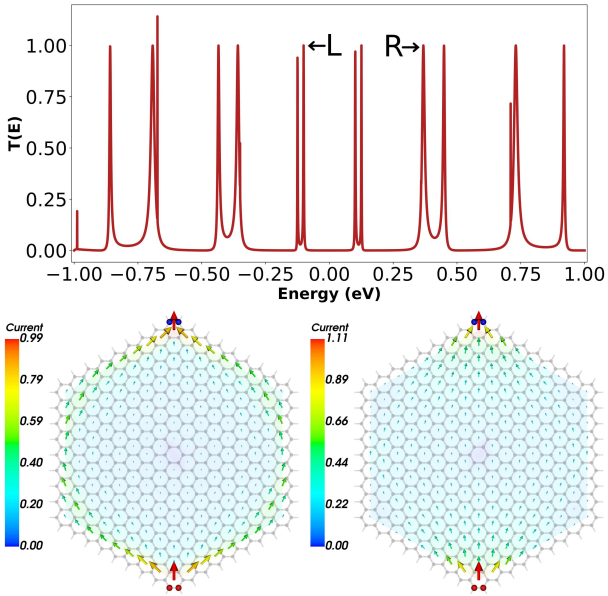


FIG. 6: Top: transmission as a function of injection energy for contacts placed at opposing vertices. Bottom: current patterns corresponding to the selected transmission peaks L (left) and R (right). The color bar presents a scale for the current intensity in units of $\frac{2e}{h}$. Contacts are represented by colored dots: source (red) and drain (blue).

As another example, we show the results for contacts placed on non-frontal edges of the hexagonal GQD. In Fig. 5b we show the transmission as a function of injection energy and two selected current patterns, corresponding to the transmission peaks indicated. Again, we see that the current follows the path of the edge states for a choice of injection energy near zero (figure on the left). An unevenly distributed vortex-like current pattern appears in the figure on the right.

Now, we investigate the case of only two contacts placed at the carbon atoms in opposing vertices, where

the edge configuration is armchair-like. Later on, in Subsection IV B, we will analyze the zigzag case. As in the previous case, in the lower part of Fig. 6 we show two representative current patterns corresponding to the selected transmission peaks shown in the upper part of the figure. As before, we see that the current, for energies near zero, follows the path of the edge states. Otherwise, it tends to spread out all over the structure. Note the mirror symmetry of both the L and R current patterns upon reflection by the axis joining the opposing contacts. Again, the symmetry of the contacts across the flake does not favor vortex formation.

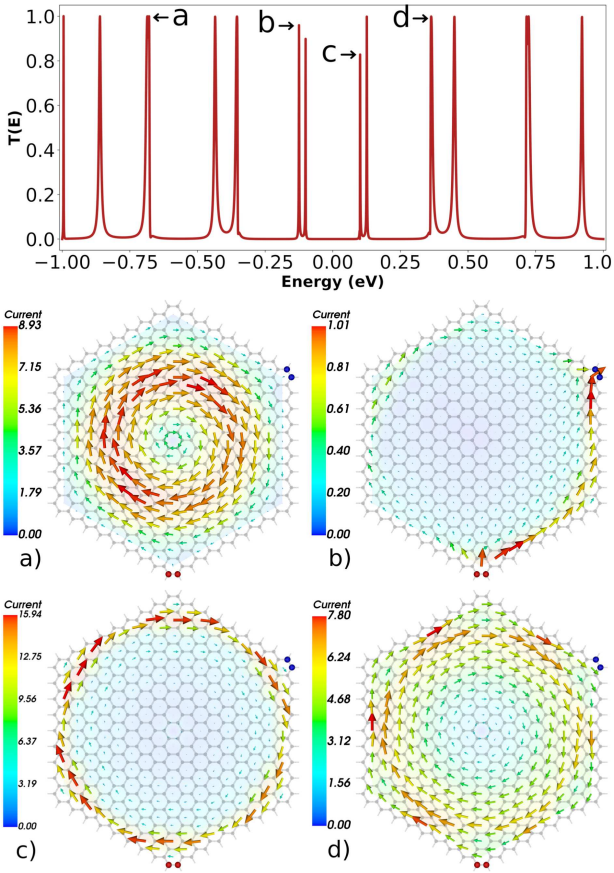


FIG. 7: Top: transmission as a function of injection energy for contacts placed at two vertices. Bottom: current patterns corresponding to the selected transmission peaks in the sequence a, b, c, d, from left to right, from top to bottom. The color bar presents a scale for the current intensity in units of $\frac{2e}{h}$. Contacts are represented by colored dots: source (red) and drain (blue).

Next, we investigate the case of non-frontal vertex contacts placed across the hexagonal GQD. In the upper part of Fig. 7 it is shown the transmission for this configuration as a function of injection energy. There, the peaks chosen for the corresponding current patterns depicted in the lower part of the figure, are indicated. Now, induced by both the non-frontal position of the contacts and the chosen energy, vortices, as well as circular edge

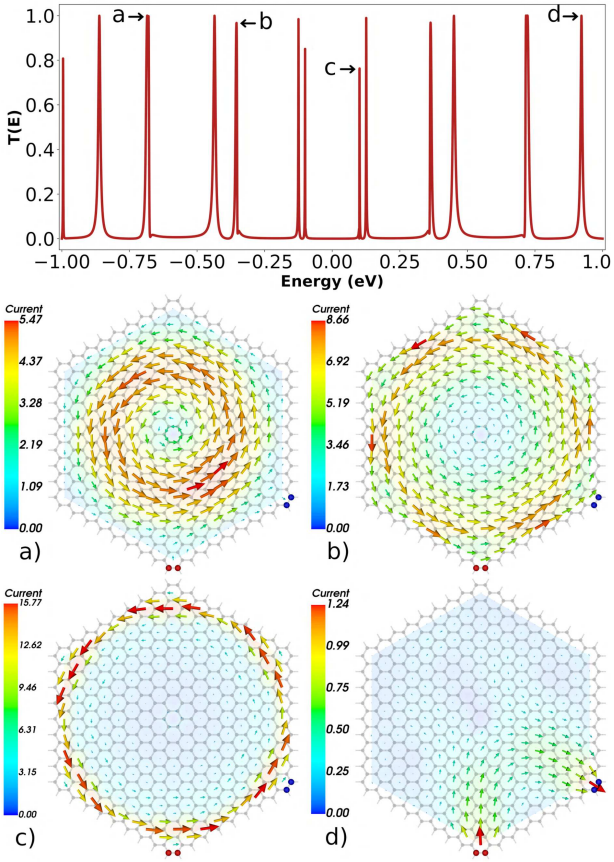


FIG. 8: Top: transmission as a function of injection energy for contacts placed at two adjacent armchair-like vertices. Bottom: current patterns corresponding to the selected transmission peaks in the sequence a, b, c, d, from left to right, from top to bottom. The color bar presents a scale for the current intensity in units of $\frac{2e}{h}$. Contacts are represented by colored dots: source (red) and drain (blue).

current, appear. Corresponding to the near zero energy peaks b and c we see, once again, the prevalence of the edge states guiding the current flow. Note, however, that only in Fig. 7c there exists a circular edge current. Comparing Figs. 6a and 7b we see that, while in the former the current splits equally over the two equivalent paths along the edge, it chooses the shorter path in the latter.

Another case, now with contacts placed at two vertices sharing the same edge, is shown in Fig. 8. Again, both vortices and circular edge current, appear. As before, the closer the injection energy is to zero, the closer the current path to the edge. It is worth commenting on the Fig. 8d: note that its injection energy is quite high, away from the small range of energy around zero that sustains edge states. Therefore, the current does not flow directly through the edge, it starts on a radial path instead, until it is attracted by the chemical potential of the second reservoir. We note that in all cases studied, the transmission peaks are of the same order of magnitude.

Nevertheless, the corresponding maximum currents may change by an order of magnitude for different injection energies. In particular, the maximum current is higher whenever a vortex appears. This apparent disagreement between transmission and maximum current is due to the fact that the transmission is related to the actual current that reaches the drain, while the maximum current is local. In other words, when a vortex is formed, a great part of the current is captured and remains circulating while only a fraction contributes to the transmission. This behavior has also been observed in current vortices in graphene nanoribbons[16]. Another way of looking at this, is to observe that the vortex is a composition of an incoming and an outgoing current, which therefore reduce the net current reaching the electrodes. According to Ref.[19], the presence of the backflow is due to quantum interference between nearly degenerate states mediated by the off-diagonal terms of the complete Hamiltonian. Also, two-atom wide contacts can only sustain a few propagating modes, which in turn limit the maximum reached by the transmission. In fact, for a perfect system, the transmission is quantized, and it grows with the width of the contacts. More on this in Sect. IV B.

IV. DISCUSSION

A. Edge effects

It is well known that the edges play an important role in the electronic properties of graphene. In graphene nanoribbons there are two possible edge types: armchair or zigzag. These conformations can also be found in other carbon-based materials such as cis-polyacetylene (armchair), trans-polyacetylene (zigzag) or nanotubes[22]. Although the bulk configuration of a graphene nanoribbon may be similar to the graphene sheet, irrespective of its edge, it is on the edge that we can find interesting electronic properties[40]. On one hand, the zigzag edge type is known to be metallic while, on the other hand, the armchair edge type is known to be either metallic or semiconducting, depending on the width of the ribbon[41]. Notice that in the cases where the current is circulating strictly on the edges, as in Figs. 7c and 8c, the maximum of the current is considerably higher than those corresponding to other contact configurations and energy peaks. This is so, due to the metallic characteristic of the zigzag edges. In fact, it was shown by Ref.[42] that at low energy the current flow is localized on the zigzag edges states, in the same sense as those depicted in Figs. 7c and 8c, which may explain the increase of the maximum of the current. Furthermore, the role of the edges states has been widely studied in several contexts[32,43–49]. Nonetheless, both armchair and zigzag edges have their importance in magnetic effects and can be used in spintronic devices as well. See, for instance,[50–53] for a detailed description.

It is also possible to suppress the edge effects by including virtual reservoirs[23] in the calculations. These

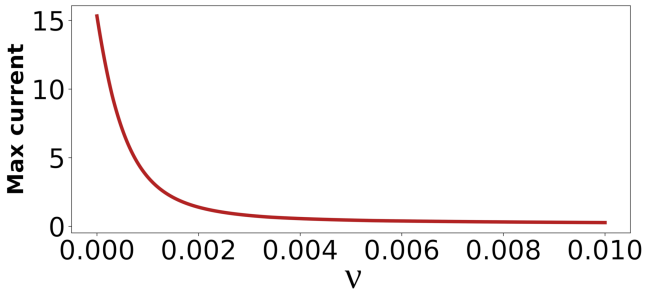


FIG. 9: Maximum current as a function of the parameter ν for the case depicted in Fig. 7c. The current is given in units of $2e/h$ and the parameter ν in eV.

are modeled using the wide-band approximation. Actually, this model is quite accurate when describing metallic contacts such as gold (for more information about the wide-band approximation, see[54]). Figure 9 shows the maximum current of Fig. 7c as a function of the parameter ν, and we can clearly see the effect of the virtual contacts, which act like absorbing boundaries, mimicking infinite dimensions of the graphene sheet[23], reducing drastically the intensity of the current and nearly extinguishing the circular flow. Naturally, the same happens in the case of Fig. 8c.

B. Effects of the contacts

In the previous section, we presented a few different cases of contact geometry on the hexagonal GQD. In each case, we used the transmission as a function of injection energy as a guide to choose the energies where there is current flowing between the contacts. Quite naturally, the complexity of the transmission profile increases with the number of contacts (see Figs. 5a and 5b) while fewer contacts lead to sharper transmission peaks (see Figs. 6, 7 and 8). This is due to the width of the reservoirs. In the case where the contact is wider, say, Figs. 5a and 5b, the transmission becomes smoother. At the contacts, the current would, in principle, be carried by an infinite number of transverse modes but, due to the limited size of the interface reservoir-GQD, only a few of these enter into the device. This is so, due to the interface resistance (see chapter 2 of Ref.[28]).

Also, it may be noticed that the maximum of the transmission in the energy range used in this work is greater for those structures with wider contacts. Again, this is due to the fact that wider contacts can carry more propagating modes. Actually, in an ideal system, the maximum number of propagating modes is proportional to the width of the contacts which leads to a quantized conductance[28,31]. When dealing with the 2-atom-wide contacts, which are the cases of Figs. 6, 7, 10 and 8, the transmission shows sharper peaks, which are a result of the short energy range where resonant states can ap-

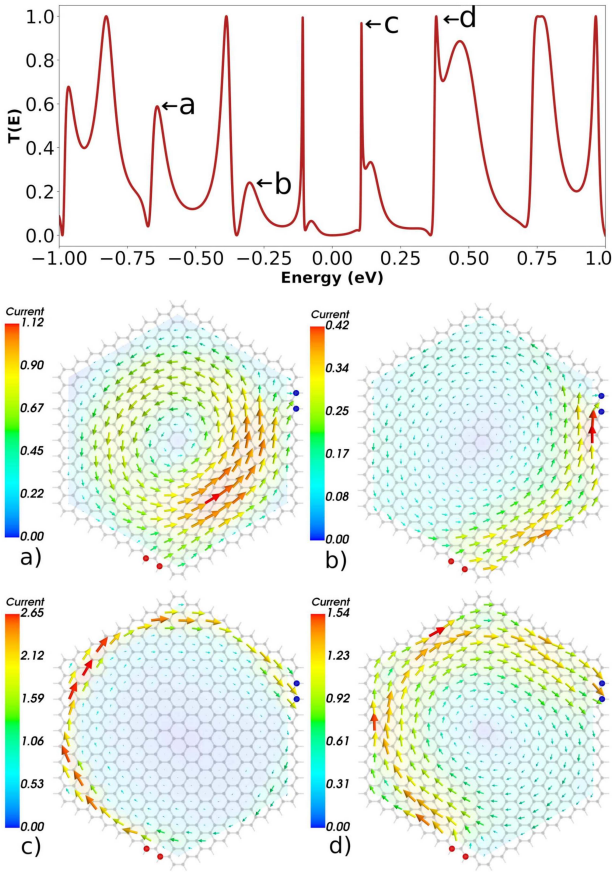


FIG. 10: Top: transmission as a function of injection energy for contacts asymmetrically placed on the zigzag edge of the hexagonal GQD. Bottom: current patterns corresponding to the selected transmission peaks in the sequence a, b, c, d, from left to right, from top to bottom. The color bar presents a scale for the current intensity in units of $\frac{2e}{h}$. Contacts are represented by colored dots: source (red) and drain (blue).

pear. It is worth mentioning that our square reservoirs can be seen as being composed of individual 1D chains and the transmission of each chain is only perfected in its conduction band, vanishing outside it. In addition, the geometry and the edge type have also a great influence on the conductance as shown by[55], when studying three-terminal systems. The break in the stepped-like conductance was also shown to appear in graphene nanoribbons with defects, both for zigzag and armchair edges[56] and in disordered graphene nanoribbons[57]. Notice that, for the cases of 2-atom-wide contacts, the transmission peaks are quasi-symmetrical with respect to zero energy and some of these symmetrical spikes give rise to similar current patterns. In all cases studied, the current patterns corresponding to transmission peaks near zero energy are dominated, not surprisingly, by the edge states. Although the edge states appear at zero energy in the free GQD (see Figs. 3 and 4 Z), with the contacts and the chemical potential difference between source and drain, the energy values where they occur are shifted from zero. For contacts placed directly in front of each other across the hexagonal GQD (see Fig. 6) there is no reason to expect current vortices, since our model does not contemplate the hydrodynamic viscous regime and the overall mirror symmetry is respected by the current flow. Indeed, we did not observe vortices in these cases. Nevertheless, when the contacts were placed at two non-frontal armchair-like vertices, which are the cases of Figs. 7 and 8 on the GQD, vortices, as well as circulating edge currents, were easily found for different injection energies. Clearly, the vortices are a consequence of the combination of the distribution of energy states around the center of the GQD, the geometry of the contacts, and the boost given to the charge carriers by the potential difference between source and drain contacts. In Fig. 7, electrons were injected and collected, respectively, at 2-atom-wide contacts placed at vertices of the GQD. There, the atoms are in an armchair configuration. When injecting electrons at contacts on the zigzag edges, like those in Fig. 10, both the vortices and edge currents become substantially modified, as can be observed comparing Figs. 7c and 10c, and Figs. 7a and 10a. The current patterns become more asymmetric and the maximum current is considerably reduced, suggesting a greater resistance at the zigzag contacts. We emphasize that it may be particularly tricky to place the contacts specifically at the GQD vertex in a real experiment. To the best of our knowledge it has not been done yet, however the production of hexagonal GQD[5–7] as well as transport measurements through GQD[58] have already been achieved.

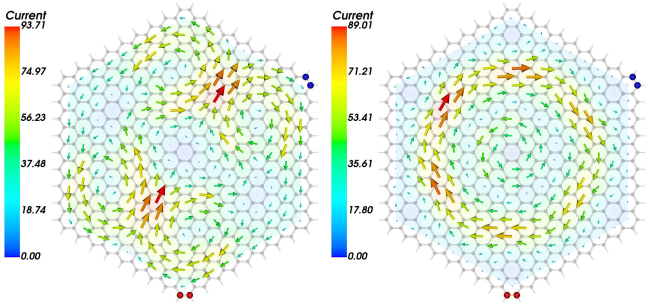


FIG. 11: Multiple-vortex patterns for two-atom-wide-contact configurations. The energies of both left and right figures are $-1.3063eV$ and $-1.6680eV$, respectively. These energies are outside the energy range showed in the inset of Fig. 3, and still form interesting current patterns. The color bar presents a scale for the current intensity in units of $\frac{2e}{h}$. Contacts are represented by colored dots: source (red) and drain (blue).

C. Symmetry effects

As remarked by Waltz and coworkers[16], in their study of current patterns in a graphene nanoribbon, "the flow

has a pronounced tendency to form ring structures (eddies) with a local current strength that exceeds the (average) through current by orders of magnitude". The regular hexagonal shape of our graphene flake leads the vortices to be concentric with the hexagon. This comes in very handy to control the placement of the magnetic flux associated to a given vortex. Nevertheless, at high injection energies, more complex current patterns appear involving multiple vortices, as shown in Fig. 11. When the source and drain are at centrosymmetric positions relative to each other across the sample, like in Fig. 6, the current distributes itself equally on both sides of the line joining the contacts. When this symmetry is broken, by placing the contacts at non-centrosymmetric positions, like in Figs 7, 8 and 11, the formation of vortices is favored. In fact, as shown in Ref.[16] the symmetry forbids the current vortices but when it is broken, they should be generic encounters. The importance of the states at energies near the injection energy of the electrons is very clear in the case of the edge currents, which are highly localized. On the other hand, the bulk currents are global, in the sense that they extend over the sample. In this case, all states will contribute, but those near the given energy contribute the most. This behavior was observed[19] in aromatic carbon molecules studied via NEGF in connection with Density Functional Theory and explained by a simple tight-binding model.

D. Edge defects and disorder

As pointed out by Aharon-Steinberg and coworkers[20] in their study of nontopological edge currents in graphene, if the current that flows on the edges is disrupted locally either by disorder or by a tip potential, at zero magnetic field the current tends to bypass the disruption through the bulk and then return to the edge. In our simulations, when the energy is close enough to zero, such as in Figs. 7d and 8b, the insertion of defects causes the current flowing in the edges to dodge the disruption. Incidentally, when symmetry is used to distribute the defects, we can also see a circular flow as shown in Fig. 12a. This can be explained by Bloch tunneling of the electrons along the periodic defect structure. However, if there is irregular-spaced disruption, disorder takes place and the constructive interference in which the circular flow is kept vanishes. It is worth mentioning that the current shown in Fig. 12a is not restricted to the edge, flowing through the bulk as well, something similar to what happens in Figs. 7d and 8b. Edge currents, as shown in Figs. 7c and 8c, were not observed in the presence of defects, irrespective if they are placed on the edge or in the bulk. In fact, when there is a defect on the structure, the density of states for zero energy is not symmetrically distributed over the edges as those shown in Fig. 4Z. The contact configuration of Fig. 12 is the same as that of Fig. 7, in order to have a clear comparison between the respective results.

Vortex-like patterns can still appear even if the defect is more pronounced, as in the case of Fig. 12b. Indeed, the vortices can appear even when the defects are in the bulk (see Fig. 12c). Interestingly, in Fig. 12b the center of the vortex does not match the center of the structure, also, the local current is more intense near the defect, which may be responsible for the shifting of the vortex.

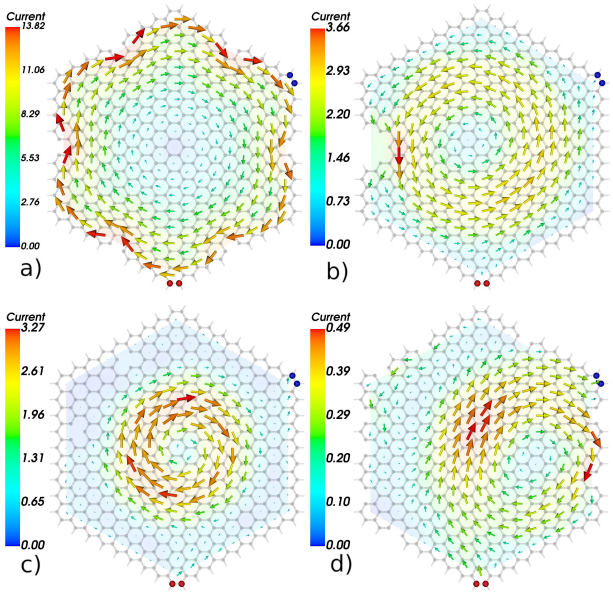


FIG. 12: Current patterns for defected structures for energies $-0.3163eV, -0.6519eV, -0.9965eV, -0.6909eV$, respectively. The hydrogen bonds in the atoms near the defect were removed from the figure in order to improve visualization. The color bar presents a scale for the current intensity in units of $\frac{2e}{h}$. Contacts are represented by colored dots: source (red) and drain (blue).

When the defects are distributed randomly in the structure, "deformed vortices" are formed, as in Fig. 12d. Notice that the maximum current of this deformed vortex is much smaller than that of the perfectly circular pattern. Also, when there is a defect, an exactly zero energy state appears both in the density of states and in the transmission, but, the respective current pattern does not show any vortex or circular flow, since it is a localized state. In fact, the effect of a single vacancy on the edges of zigzag graphene nanoribbons can change the characteristic of the edges from metallic to semiconducting, due to localization. See[59,60] for more information on the effect of disorder and vacancies in graphene nanoribbons.

V. CONCLUDING REMARKS

The results presented here testify to the important role of contact geometry in the electronic properties of graphene quantum dots. When the position of the contacts are placed at centrosymmetric positions across the

GQD, the current follows a direct path between the source and drain contacts. The path broadens and approaches the edge due to the increased importance of the edge states when the injection energy nears zero. Current vortices and circular edge currents appear when the centrosymmetry is broken and the contacts are placed in non-frontal armchair-like vertices on the GQD. Also, in the presence of the disorder introduced by defects, the edge currents do not appear. However, the bulk current that forms vortices seems to be robust even when there are few defects. We point out that, when one has several defects, either on the edges or in the bulk, the edge circular current is destroyed and the intensity of the current of bulk vortices that may be formed is substantially reduced. But, when the defects are distributed periodically over the edge, the edge current is maintained by Bloch tunneling. Such current vortices can be used in the design of quantum devices[61], since their currents give rise to an extremely concentrated magnetic field. These currents can also be used to generate spin-based quantum devices, since the orientation of a spin placed at the center of the vortex can be manipulated by the induced magnetic field[62]. Conversely, the current vortex will be affected by external magnetic perturbations in its proximity. This suggests the use of GQD, both as nanomagnets and as magnetic nanosensors. These might have applications in nanoscale magnetic recording or in electron microscopy, for instance. Another possible application is in the design of energy-tunable electron[63] or even plasmonic[64] lenses. Another interesting related subject is the study of magnetic textures associated to the multivortices. The study of current vortices in differently shaped quantum dots is currently being performed in our group, including both geometrical and topological deformations. We can anticipate that other geometries and shapes sustain such currents as well, which increases the possibility of experimental verification of these results.

VI. ACKNOWLEDGMENTS

This work was supported by the Brazilian agencies Fundação de Amparo à Ciência e Tecnologia do Estado de Pernambuco (FACEPE), Grant No. BIC-1187-1.05/20 (E.G.), and Conselho Nacional de Desenvolvimento Científico e Tecnológico (CNPq), Grant No. 307687/2017-1 (F.M.). We also thank Dr. Denis R. Candido for invaluable discussions.

* eudes.gomes@ufrpe.br
† fernando.jsmoraes@ufrpe.br

[1] M. Bacon, S. J. Bradley, and T. Nann, Particle & Particle Systems Characterization **31**, 415 (2014).
[2] K. Nishigaya, K. Kishibe, and K. Tanabe, C—Journal of Carbon Research **6**, 28 (2020).
[3] S.-H. Choi, Journal of Physics D: Applied Physics **50**, 103002 (2017).
[4] Y. J. Chung, J. Kim, and C. B. Park, ACS nano **14**, 6470 (2020).
[5] C. D. Simpson, J. D. Brand, A. J. Berresheim, L. Przybilla, H. J. Räder, and K. Müllen, Chemistry–A European Journal **8**, 1424 (2002).
[6] P. Egberts, G. H. Han, X. Z. Liu, A. C. Johnson, and R. W. Carpick, ACS nano **8**, 5010 (2014).
[7] S. H. Lee, D. Y. Kim, J. Lee, S. B. Lee, H. Han, Y. Y. Kim, S. C. Mun, S. H. Im, T.-H. Kim, and O. O. Park, Nano letters **19**, 5437 (2019).
[8] M. Zarenia, A. Chaves, G. Farias, and F. Peeters, Physical Review B **84**, 245403 (2011).
[9] S. Ghosh and U. Schwingenschlögl, physica status solidi (RRL)–Rapid Research Letters **11**, 1600226 (2017).
[10] L. Levitov and G. Falkovich, Nature Physics **12**, 672 (2016).
[11] S. Danz and B. N. Narozhny, 2D Materials **7**, 035001 (2020).
[12] A. Lucas and K. C. Fong, Journal of Physics: Condensed Matter **30**, 053001 (2018).
[13] D. Bandurin, I. Torre, R. K. Kumar, M. B. Shalom, A. Tomadin, A. Principi, G. Auton, E. Khestanova, K. Novoselov, I. Grigorieva, *et al.*, Science **351**, 1055 (2016).
[14] A. Levin, G. Gusev, E. Levinson, Z. Kvon, and A. Bakarov, Physical Review B **97**, 245308 (2018).
[15] A. Gupta, J. Heremans, G. Kataria, M. Chandra, S. Fallahi, G. Gardner, and M. Manfra, Physical Review Letters **126**, 076803 (2021).
[16] M. Walz, J. Wilhelm, and F. Evers, Physical review letters **113**, 136602 (2014).
[17] T. Stuyver, N. Blotwijk, S. Fias, P. Geerlings, and F. De Proft, ChemPhysChem **18**, 3012 (2017).
[18] M. Ernzerhof, H. Bahmann, F. Goyer, M. Zhuang, and P. Rocheleau, Journal of chemical theory and computation **2**, 1291 (2006).
[19] T. Stegmann, J. A. Franco-Villafañe, Y. P. Ortiz, M. Deffner, C. Herrmann, U. Kuhl, F. Mortessagne, F. Leyvraz, and T. H. Seligman, Physical Review B **102**, 075405 (2020).
[20] A. Aharon-Steinberg, A. Marguerite, D. J. Perello, K. Bagani, T. Holder, Y. Myasoedov, L. S. Levitov, A. K. Geim, and E. Zeldov, Nature **593**, 528 (2021).
[21] T. Li and S.-P. Lu, Physical Review B **77**, 085408 (2008).
[22] G. Dresselhaus, M. S. Dresselhaus, and R. Saito, *Physical properties of carbon nanotubes* (World scientific, 1998).
[23] T. Stegmann and N. Szpak, New Journal of Physics **18**, 053016 (2016).
[24] T. Stegmann and N. Szpak, 2D Materials **6**, 015024 (2018).
[25] S. Datta, Superlattices and microstructures **28**, 253 (2000).
[26] H. Schomerus, Physical review B **76**, 045433 (2007).
[27] S.-M. Dubois, Z. Zanolli, X. Declerck, and J.-C. Charlier, The European Physical Journal B **72**, 1 (2009).
[28] S. Datta, *Electronic transport in mesoscopic systems* (Cambridge university press, 1997).

[29] S. Datta, *Quantum transport: atom to transistor* (Cambridge university press, 2005).
[30] C. H. Lewenkopf and E. R. Mucciolo, Journal of Computational Electronics **12**, 203 (2013).
[31] T. Stegmann, *Quantum transport in nanostructures: From the effects of decoherence on localization to magnetotransport in two-dimensional electron systems*, Ph.D. thesis, Universität Duisburg-Essen (2014).
[32] T. Stegmann, D. E. Wolf, and A. Lorke, New Journal of Physics **15**, 113047 (2013).
[33] P. Schmitteckert, Journal of Physics: Conference Series **220**, 012022 (2010).
[34] P. Ramachandran and G. Varoquaux, Computing in Science & Engineering **13**, 40 (2011).
[35] S. E. Stein and R. Brown, Journal of the American Chemical Society **109**, 3721 (1987).
[36] P. Ulloa, A. Latgé, L. E. Oliveira, and M. Pacheco, Nanoscale research letters **8**, 384 (2013).
[37] M. Wimmer, A. Akhmerov, and F. Guinea, Physical Review B **82**, 045409 (2010).
[38] A. Zhou and W. Sheng, Journal of Applied Physics **112**, 094313 (2012).
[39] R. Pohle, E. G. Kavousanaki, K. M. Dani, and N. Shannon, Physical Review B **97**, 115404 (2018).
[40] L. Malysheva and A. Onipko, Physical review letters **100**, 186806 (2008).
[41] K. Wakabayashi, K. ichi Sasaki, T. Nakanishi, and T. Enoki, Science and Technology of Advanced Materials **11**, 054504 (2010).
[42] J. Mabillard, T. Can, and D. K. Morr, New Journal of Physics **16**, 013054 (2014).
[43] A. Uri, Y. Kim, K. Bagani, C. K. Lewandowski, S. Grover, N. Auerbach, E. O. Lachman, Y. Myasoedov, T. Taniguchi, K. Watanabe, *et al.*, Nature Physics **16**, 164 (2020).
[44] Z.-F. Liu, Q.-P. Wu, A.-X. Chen, X.-B. Xiao, N.-H. Liu, and G.-X. Miao, Scientific reports **7**, 1 (2017).
[45] X. Ji, J. Zhang, Y. Wang, H. Qian, and Z. Yu, Nanoscale **5**, 2527 (2013).
[46] M. Zhu, A. Kretinin, M. D. Thompson, D. Bandurin, S. Hu, G. Yu, J. Birkbeck, A. Mishchenko, I. J. Vera-Marun, K. Watanabe, *et al.*, Nature communications **8**, 1 (2017).
[47] T. Christensen, W. Wang, A.-P. Jauho, M. Wubs, and N. A. Mortensen, Physical Review B **90**, 241414 (2014).
[48] A. Pramanik, B. Mandal, S. Sarkar, and P. Sarkar, Chemical Physics Letters **597**, 1 (2014).
[49] S. Fujii, M. Ziatdinov, M. Ohtsuka, K. Kusakabe, M. Kiguchi, and T. Enoki, Faraday discussions **173**, 173 (2014).
[50] R. Farghadan, A. Saffarzadeh, and E. Heidari Semiromi, Journal of Applied Physics **114**, 214314 (2013).
[51] R. Farghadan and E. Saievar-Iranizad, Journal of Applied Physics **111**, 014304 (2012).
[52] A. Saffarzadeh and R. Farghadan, Applied Physics Letters **98**, 023106 (2011).
[53] R. Farghadan and M. Yoosefi, Physica E: Low-dimensional Systems and Nanostructures **83**, 414 (2016).
[54] C. Verzijl, J. Seldenthuis, and J. Thijssen, The Journal of chemical physics **138**, 094102 (2013).
[55] V. Torres, D. Faria, and A. Latgé, Physical Review B **97**, 165429 (2018).
[56] N. Gorjizadeh, A. A. Farajian, and Y. Kawazoe, Nanotechnology **20**, 015201 (2008).
[57] E. R. Mucciolo, A. C. Neto, and C. H. Lewenkopf, Physical Review B **79**, 075407 (2009).
[58] J. Güttinger, F. Molitor, C. Stampfer, S. Schnez, A. Jacobsen, S. Dröscher, T. Ihn, and K. Ensslin, Reports on Progress in Physics **75**, 126502 (2012).
[59] D. A. Areshkin, D. Gunlycke, and C. T. White, Nano letters **7**, 204 (2007).
[60] M. Poljak, E. B. Song, M. Wang, T. Suligoj, and K. L. Wang, IEEE transactions on electron devices **59**, 3231 (2012).
[61] D. Rai, O. Hod, and A. Nitzan, The Journal of Physical Chemistry C **114**, 20583 (2010).
[62] S. Saha, S. K. Maiti, and S. Karmakar, Physics Letters A **380**, 1741 (2016).
[63] L. Gerhard, E. Moyen, T. Balashov, I. Ozerov, M. Portail, H. Sahaf, L. Masson, W. Wulfhekel, and M. Hanbücken, Applied Physics Letters **100**, 153106 (2012).
[64] D. Smirnova, S. H. Mousavi, Z. Wang, Y. S. Kivshar, and A. B. Khanikaev, ACS Photonics **3**, 875 (2016).